Journal of Pharmaceutical Analysis 11 (2021) 163–173

Contents lists available at ScienceDirect

Journal of Pharmaceutical Analysis

journal homepage: www.elsevier.com/locate/jpa

Original article

Design and preparation of a new multi-targeted drug delivery system using multifunctional nanoparticles for co-delivery of siRNA and paclitaxel

Sara Hosayni Nasab [a], Amin Amani [a, b], Hossein Ali Ebrahimi [c, *], Ali Asghar Hamidi [d]

[a] Department of Agronomy and Plant Breeding, Faculty of Agriculture and Natural Resources, University of Mohaghegh Ardabili, Ardabil, Iran
[b] Biotechnology Research Center, Tabriz University of Medical Sciences, Tabriz, Iran
[c] Department of Pharmaceutics, School of Pharmacy, Ardabil University of Medical Sciences, Ardabil, Iran
[d] Department of Medicinal Chemistry, Faculty of Pharmacy, Tabriz University of Medical Sciences, Tabriz, Iran

ARTICLE INFO

Article history:
Received 16 December 2019
Received in revised form
7 April 2020
Accepted 17 April 2020
Available online 23 April 2020

Keywords:
Paclitaxel
siRNA
Targeted drug delivery
Magnetic nanoparticles
Polymeric drug delivery

ABSTRACT

Drug resistance is a great challenge in cancer therapy using chemotherapeutic agents. Administration of these drugs with siRNA is an efficacious strategy in this battle. Here, the present study tried to incorporate siRNA and paclitaxel (PTX) simultaneously into a novel nanocarrier. The selectivity of carrier to target cancer tissues was optimized through conjugation of folic acid (FA) and glucose (Glu) onto its surface. The structure of nanocarrier was formed from ternary magnetic copolymers based on FeCo-polyethyleneimine (FeCo-PEI) nanoparticles and polylactic acid-polyethylene glycol (PLA-PEG) gene delivery system. Biocompatibility of FeCo-PEI-PLA-PEG-FA(NPsA), FeCo-PEI-PLA-PEG-Glu (NPsB) and FeCo-PEI-PLA-PEG-FA/Glu (NPsAB) nanoparticles and also influence of PTX-loaded nanoparticles on in vitro cytotoxicity were examined using MTT assay. Besides, siRNA-FAM internalization was investigated by fluorescence microscopy. The results showed the blank nanoparticles were significantly less cytotoxic at various concentrations. Meanwhile, siRNA-FAM/PTX encapsulated nanoparticles exhibited significant anticancer activity against MCF-7 and BT-474 cell lines. NPsAB/siRNA/PTX nanoparticles showed greater effects on MCF-7 and BT-474 cells viability than NPsA/siRNA/PTX and NPsB/siRNA/PTX. Also, they induced significantly higher anticancer effects on cancer cells compared with NPsA/siRNA/PTX and NPsB/siRNA/PTX due to their multi-targeted properties using FA and Glu. We concluded that NPsAB nanoparticles have a great potential for co-delivery of both drugs and genes for use in gene therapy and chemotherapy.

1. Introduction

Cancer has been identified as the second main cause of mortality worldwide, after heart diseases [1]. Chemotherapy, one of the most common treatment procedures for cancer therapy, is used after surgery and in a combination with radiotherapy [2]. Although the chemotherapy has been proved to be useful in many cases, the severity of its side effects and also the drug resistance to these drugs reduce the efficacy of chemotherapeutic agents [3].

During the previous few decades, nanoparticles were employed to optimize the effect of drugs and genes, reduce their side effects and deliver the medicines in a targeted manner for efficient therapy [4]. Folic acid (FA) is an essential nutrient for the human body which can enter cells through folate receptors (FRs) [5]. In the human body, FA is used in the synthesis of the DNA. Therefore, the expression level of FR in cancer cells is higher than that of normal cells, due for theirs need for high level of FA [6,7].

Glucose (Glu) is another important nutrient in human body which provides the energy needed in many metabolic functions and synthetic processes of different compounds in cells, serum and tissues [8]. Therefore, glucose transporters (Gluts) are over expressed on the cell membrane of many malignant cells [9,10]. In 1927, Warburg et al. [11] reported that Glu uptake was significantly enhanced in cancer tissues compared to those in normal tissues because of their high metabolic activity. Since that, Glu has been used to target cancer cells for different diagnostic and therapeutic

Peer review under responsibility of Xi'an Jiaotong University.
* Corresponding author.
E-mail address: h.ebrahimi@pharmacy.arums.ac.ir (H.A. Ebrahimi).

https://doi.org/10.1016/j.jpha.2020.04.005

applications [12,13].

It is well known that the targeted endocytosis pathway of nanoparticles is based on the interaction between cell surface receptors and ligands [14]. Therefore, the efficiency of drug delivery was limited up to saturation of cell surface receptors by specific ligands of nanoparticles. Therefore, it seems that specific targeting of tumor tissues could be improved through simultaneous incorporation of several ligands such as Glu and FA inside the structure of nanoparticles. So, in this study it was aimed to optimize the surface of nanoparticles with co-addition of FA and Glu.

In recent years, drug resistance has emerged as one of the biggest therapeutic challenges in cancer therapy, so it has attracted much research attention [15,16]. Simultaneous co-targeting of cancer cells using two or more drugs seems to be a novel and effective approach to overcoming the problem of drug resistance [17–19]. The use of siRNA to suppress expression of oncogenes has been considered as a promising solution for cancer treatment in recent years [20,21]. Although this method can be helpful in itself, due to the complexity of human cancer, other complementary therapies may be needed to improve the efficacy of cancer therapy by siRNA [22,23]. Combination therapy of siRNA and chemotherapeutics such as PTX has been considered as a useful strategy for increasing the effectiveness of cancer therapy [24].

Various carriers are used to deliver genetic agents. Cationic polymers such as polyethyleneimine (PEI) are of the most common ones and have the ability to interact with RNA and DNA and form complexes with high transfection efficiency. However, studies show that application of PEI is associated with critical cytotoxicity effects [25,26]. In addition, hydrophilic polymers such as PEI have low capacity as a nano-vector for delivering hydrophobic and neutral drugs such as PTX into cancer cells. Several methods have been developed to transfer different compounds using nanoparticles to cancer cells [27,28]. Synthesis of copolymers by binding of hydrophobic polymers such as polylactide acid (PLA) to cationic hydrophilic polymers allows simultaneous co-delivery of siRNA and PTX to cancer cells [29–32].

Biodegradable polymers such as PLA, poly(D,L-lactide-co-glycolide) (PLGA) and polyglycolide (PGA) have a great application potential as drug carriers due to their good biocompatibility and biodegradability [33–35].

Researchers have developed tri-block copolymers using PLA, PEI, and polyethylene glycol (PEG) such as tri-block PEI-PLA-PEG copolymers, as potential gene delivery nano-vectors [36]. The hydrophobic PLA segment affords a degree of biodegradability to nanoparticles. It also increases the stability of nano-carrier through charge shielding effects. In recent decades, much study has been done on multifunctional nanoparticle. Multifunctional nanoparticles are attractive for cancer treatment due to high potential to overcome the barriers in various extracellular and intracellular conditions [37–39]. This study presents multifunctional biodegradable magnetic nanoparticles including PLA, PEG, PEI, FeCo nanoparticles, FA and Glu for co-delivery and targeting of siRNA and PTX.

2. Materials and methods

2.1. Materials

2-azidoethyl β-D-galactopyranoside was purchased from Synthose Inc. (Canada); polyethyleneimine (PEI, MW 1800 Da) was purchased from Polysciences, Inc. (Warrington, PA, USA); stannous octoate, tetraethyl orthosilicate (TEOS), 1-ethyl-3-(3-dimethylaminopropyl) carbodiimide (EDC), polyvinyl alcohol (PVA), dichloromethane (DCM), MTT, RPMI 1640, dimethyl sulfoxide (DMSO), penicillin/streptomycin solution, N-hydroxylsulfosuccinimide (NHS), and fetal bovine serum (FBS) were purchased from Sigma-Aldrich (USA). OH-PEG-COOH was obtained from Rapp Polymere GmbH (Germany). N-hydroxysuccinimide, FA and dicyclohexylcarbodiimide were purchased from Acros (Germany). Agarose gel, polyvinyl pyrrolidone (PVP), $MgCl_2$, Tris-HCl, and ethylene diamine tetraacetic acid (EDTA) were purchased from Merck (Germany).

2.2. Synthesis of azido-functionalized folate

Preparation of PLA-PEG-FA copolymer was started with the synthesis of OH-PLA-PEG-COOH according to the method described by Hami et al. [4]. Briefly, definite amounts of lactide monomers were added to OH-PEG-COOH under dry argon; then the reaction was continued at 140 °C for 24 h in the presence of stannous octoate ($Sn(Oct)_2$) as catalyst. The mixture was dissolved in chloroform and precipitated by a mixture of ether and methanol (1:1, *V*/*V*). Then, the OH-PLA-PEG-COOH obtained as precipitate was dried. This obtained polymer was dissolved in DCM with N,N'-dicyclohexylcarbodiimide (DCC) (1.2 mmol) and NHS (0.6 mmol). The product was stirred at 0 °C and 25°C for 1 h and 24 h, respectively. Triethylamine (TEA) and propargylamine (0.6 mmol) were added into the above product. Next, the mixture was stirred at 25°C for another 24 h. The product (OH-PLA-PEG-alkyne copolymer) was precipitated in cold ether, filtered and dried at 30 °C under vacuum. Then, the OH-PLA-PEG-alkyne copolymer (0.1 mmol) was conjugated with acryloyl chloride (C_3H_3ClO, 0.2 mmol) in dry toluene containing triethylamine ($C_6H_{15}N$, 0.2 mmol). The sample was stirred for 10 h at 80 °C. After that, the product was cooled to 25°C, filtered and precipitated in n-hexane then dried in vacuum oven to produce acrylate-PLA-PEG-alkyne copolymer. Acrylate-PLA-PEG-FA and acrylate-PLA-PEG-Glu were synthesized stepwise by the addition of acrylate-PLA-PEG-alkyne copolymer (0.1 mmol) and azido-functionalized folate and azido-functionalized Glu in 30 mL of aqueous NH_4HCO_3 (10 mM) separately. Then, sodium ascorbate and $CuSO_4$ solutions were added to acrylate-PLA-PEG-alkyne copolymer and stirred with a rotator at 25 °C for 24 h. Next, the product was filtered with a 0.22 μm membrane filter. The reaction solutions were diluted with sufficient NaCl aqueous solution, and then extracted several times by dichloromethane. The resulting products were concentrated under vacuum and precipitated in cold ether. Finally, acrylate-PLA-PEG-FA copolymer and acrylate-PLA-PEG-Glu copolymers were dried under vacuum.

2.3. Synthesis of FeCo nanoparticles

First, FeO(OH) and Co_3O_4 in appropriate amount were dissolved in trioctylamine (TOA); then the mixture was loaded into a flask and dehydrated at 160 °C for 2 h under a flow of argon. Afterwards, the mixture was quickly heated to 370 °C while vigorous stirring was maintained using a mechanical stirrer. Next, the product was cooled to room temperature and collected by centrifugation at 10,000 rpm. Finally, the product was washed with hexane and ethanol, and dried under vacuum to obtain FeCo nanoparticles (FeCo NPs).

2.4. Synthesis of FeCo@SiO_2-SS-PEI nanoparticles

To synthesize the FeCo@SiO_2-SH, 200 mg of FeCo NPs dispersed in ethanol by ultrasound, followed by sequential addition of 1 mL $NH_3 \cdot H_2O$, 20 mL TEOS and 1 mL mercaptopropyltrimethoxysilane (MPTMS) in the ultrasound for 3 h [41].

Then, the nanoparticles were collected using magnet and washed with ethanol and water for 5 times, and then the magnetic nanoparticles were dried under vacuum at 25 °C. To synthesize FeCo@SiO_2-SS-COOH nanoparticles, 200 mg of sulfhydrylated

FeCo NPs was dispersed in 12 mL methanol, and then, the 2-carboxyethyl 2-pyridyl disulfide (200 mg) was added and reaction performed for 36 h; the obtained nanoparticles were washed and then dried as mentioned above. Finally, to synthesize FeCo@SiO_2-SS-PEI nanoparticles, 200 mg of FeCo@SiO_2-SS-COOH nanoparticles was dispersed in 16 mL PBS buffer (pH = 7.4) and subsequently the activation of the carboxyl groups was performed with addition of 200 mg EDC and 100 mg NHS at 25 °C for 90 min. After that, 4 mL PBS buffer containing 200 mg PEI (1800 Da) was added and stirred at 25 °C for 2 days. The resulting nanoparticles were washed with distilled water and ethanol; then the nanoparticles were lyophilized (Lifilizator Alpha model 1-2 LD plus, Christ, Germany).

2.5. Synthesis of FeCo@SiO_2-SS-PEI-PLA-PEG-FA and FeCo@SiO_2-SS-PEI-PLA-PEG-Glu and FeCo@SiO_2-SS-PEI-PLA-PEG-Glu-FA

FeCo@SiO_2-SS-PEI, acrylate-PLA-PEG-FA and acrylate-PLA- PEG-Glu were dissolved in 6 mL of chloroform, separately. The chloroform solution of acrylate-PLA-PEG-FA and acrylate-PLA-PEG-Glu was added dropwise into FeCo@SiO_2-SS-PEI solution separately. Then the mixture was stirred for 24 h at 45 °C and stirred for 24 h. The resulting nanoparticles were washed with distilled water and ethanol; then the dispersion was centrifuged at 11068 *g* for 30 min and the supernatant was removed. Finally, the nanoparticles were lyophilized. To synthesize FeCo@SiO_2-SS-PEI-PLA-PEG-Glu-FA nanoparticles, the same amounts of acrylate-PLA-PEG-FA and acrylate-PLA-PEG-Glu were added into FeCo@SiO_2-SS-PEI solution. Then the FeCo@SiO_2-SS-PEI-PLA-PEG-Glu-FA nanoparticles were synthesized as protocol mentioned above.

2.6. Encapsulation of siRNA-FAM and PTX into NPsA, NPsB and NPsAB

The drug-loaded nanoparticles NPsA/siRNA/PTX, NPsB/siRNA/PTX and NPsAB/siRNA/PTX were prepared based on the previous report with minor modification [42].

Briefly, to synthesize NPsA/siRNA/PTX, 0.5 mL water solution containing siRNA-FAM (250 μg) was added dropwise into 4 mL of aceton/DCM solution containing NPsA (30 mg) and PTX (5 mg). The reaction mixture was sonicated on ice for 30 s (Sonicator® XL, Misonix, NY, USA), then slowly added to 6 mL of 1% (*m/V*) PVA solution and sonicated again for 2 min. Next, the reaction mixture was poured dropwise into a stirred PVA solution (30 mL, 0.3% (*m/V*)).

After 5 min, the solvent (DCM and acetone) from the nanoparticles fraction was evaporated using a rotary vacuum evaporator. Then, the NPsA/siRNA/PTX were collected were collected from the solution by centrifugation at 15000 rpm (16602 *g*) for 30 min (Sigma 1–14K), and after washed several times with deionized water to remove the unloaded drug, the resultant was filtered using 0.1 and 0.45 μm membrane filters to remove large scattering particles and free NPsA, and finally, the product was lyophilized. The NPsB/siRNA/PTX and NPsAB/siRNA/PTX were also prepared as described above.

The encapsulation efficiency of siRNA-FAM and PTX in nanoparticles was determined by measuring the amount of siRNA-FAM and PTX that was not encapsulated in nanoparticles. Therefore, the amounts of siRNA-FAM and PTX in the supernatant of the nanoparticles were measured using spectrophotometer at 490 (siRNA-FAM) and 230 (PTX) nm, respectively [43,44]. Then, the amount of siRNA-FAM and PTX in the supernatant was compared with the total amount of siRNA-FAM and PTX used in the encapsulation process [45].

Encapsulation efficiency (EE) of siRNA-FAM and PTX was determined with the following Eq. (1):

$$EE\,(\%) = \frac{\text{Amount of used drug} - \text{Amount of drug in supernatant}}{\text{Amount of used drug}} \times 100 \quad (1)$$

The PTX and siRNA release kinetics from the nanoparticles was assessed in PBS buffer (pH 7.4). The nanoparticles were treated separately with 5 mL of PBS buffer (1 mg/mL) then, collected via centrifugation (16602 *g* for 30 min) at predetermined time intervals (i.e., 30 min-30 days after inoculation). After each collection, the supernatants were employed to determine the amount of siRNA and PTX released from the nanoparticles. Afterwards, nanoparticles were re-suspended in 5 mL of fresh PBS buffer (pH 7.4), and incubated at 37 °C until the next scheduled time interval. The total drug release ratio for each sample was calculated using the following Eq. (2):

$$\text{Cumulative release}\ (\%) = \frac{\text{Total drug content in supernatant}}{\text{The amount of encapsulated drug}} \times 100 \quad (2)$$

The optical density of samples was measured after calibration of spectrophotometer with blank sample (the nanoparticles without drug).

2.7. Characterization of nanoparticles

In the present study, transmission electron microscopy (TEM; JEM-2100, JEOL, Tokyo, Japan) was used to characterize the morphology of nanoparticles.

The average size, zeta potential and magnetic properties of nanoparticles were investigated using dynamic light scattering (DLS, Malvern Instruments, Westborough, MA, USA) and vibrating sample magnetometer (VSM, a Standard 7403 Series, Lakeshore), respectively.

2.8. In vitro cytotoxicity and transfection assay

The in vitro cytotoxicity assay for blank nanoparticles (NPsA, NPsB and NPsAB) and siRNA-FAM/PTX encapsulated nanoparticles (NPsA/siRNA/PTX, NPsB/siRNA/PTX and NPsAB/siRNA/PTX) was evaluated on MCF-7 and BT-474 cell lines. The cells were seeded in 96-well plates at a density of approximately 7000 cells per well, in 100 μL of complete growth medium (RPMI 1640 culture medium supplemented with 1% penicillin/streptomycin and 10% FBS) and were incubated at 37°C in 5% CO_2 for 24 h. Then the cells were exposed to various concentrations of the blank nanoparticles (100, 200, 400, 600, 800 and 1000 μg/mL) for 48 h at 37°C. Next, each well was supplemented with 20 μL of MTT solution (5 μg/mL in culture medium) for 5 h at 37°C. The supernatant was removed and 200 μL of DMSO was added per well to dissolve the formazan crystals. Following this step, the plates were incubated at 37°C for 30 min. Next, the absorbance level at 570 nm was recorded by a multiwall plate reader (BioTek Instruments, Winooski, VT, USA) [46]. Finally, the percentage for the cell viability was determined according to the following Eq. (3):

$$\text{Cell viability}\ (\%) = \frac{\text{OD of each sample at 570 nm}}{\text{OD of negative control at 570 nm}} \times 100 \quad (3)$$

In order to investigate the anti-cancer effects of the nanoparticles encapsulated with siRNA-FAM/PTX (NPsA/siRNA/PTX, NPsB/siRNA/PTX and NPsAB/siRNA/PTX) against the MCF-7 and BT-

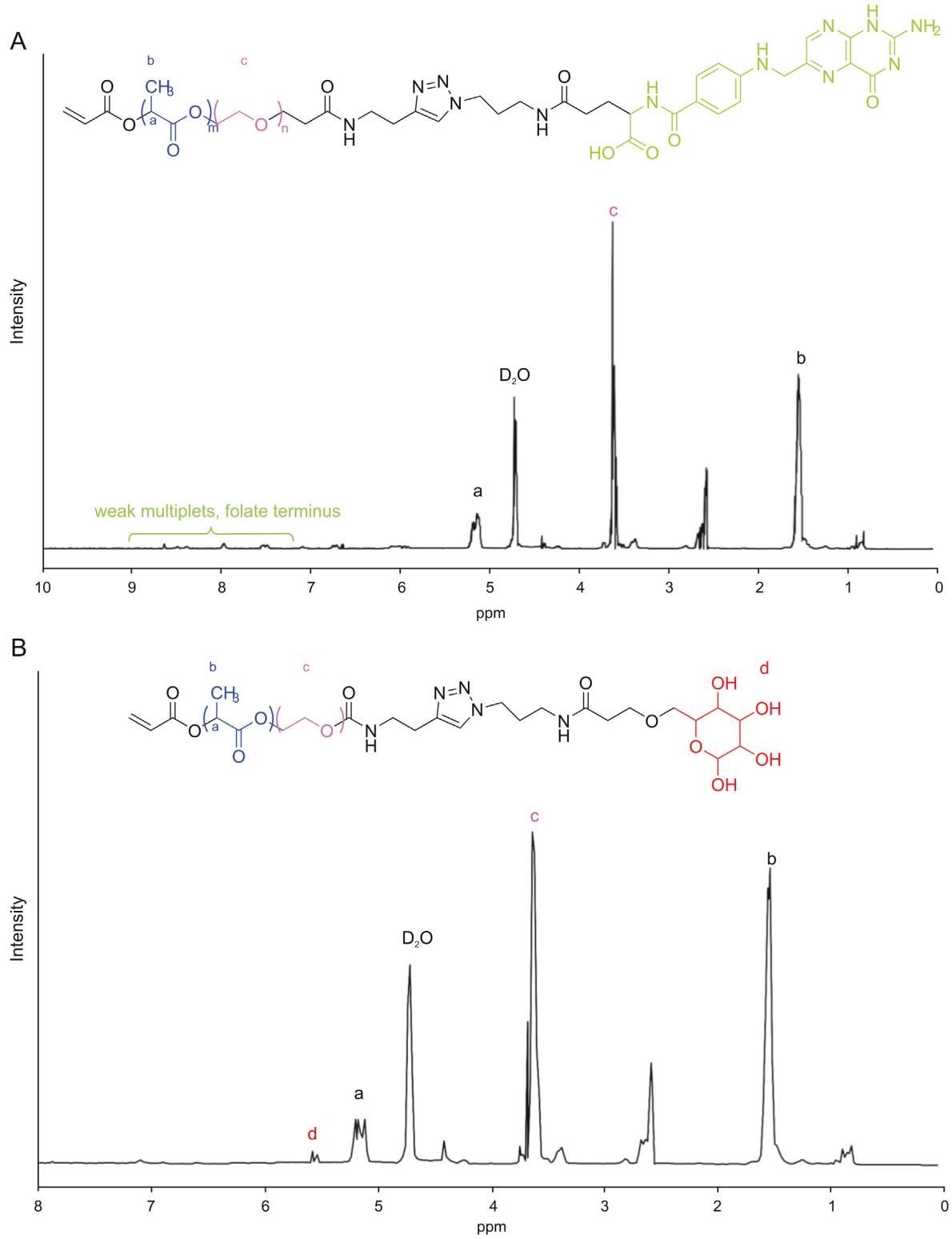

Fig. 1. ^{1}H NMR spectra of (A) PLA-PEG-FA and (B) PLA-PEG-Glu in D_2O solvent. PLA: polylactic acid; PEG: polyethylene glycol; FA: folic acid; Glu: glucose.

474 cell lines, an appropriate amount of the nanoparticles containing different concentrations of PTX (10, 20, 40, 60 and 80 nM) was poured to each well of 96-well microtiter plates. The viability of MCF-7 and BT 474 cells was evaluated as mentioned above after incubation at 37 for 48 h. To investigate the transfection ability of nanoparticles, the cells were incubated with NPsA/siRNA/PTX, NPsB/siRNA/PTX and NPsAB/siRNA/PTX, then were washed twice using PBS, and the siRNA-FAM transfection efficiency was determined using an inverted-fluorescent microscope (Nikon TE200, Japan).

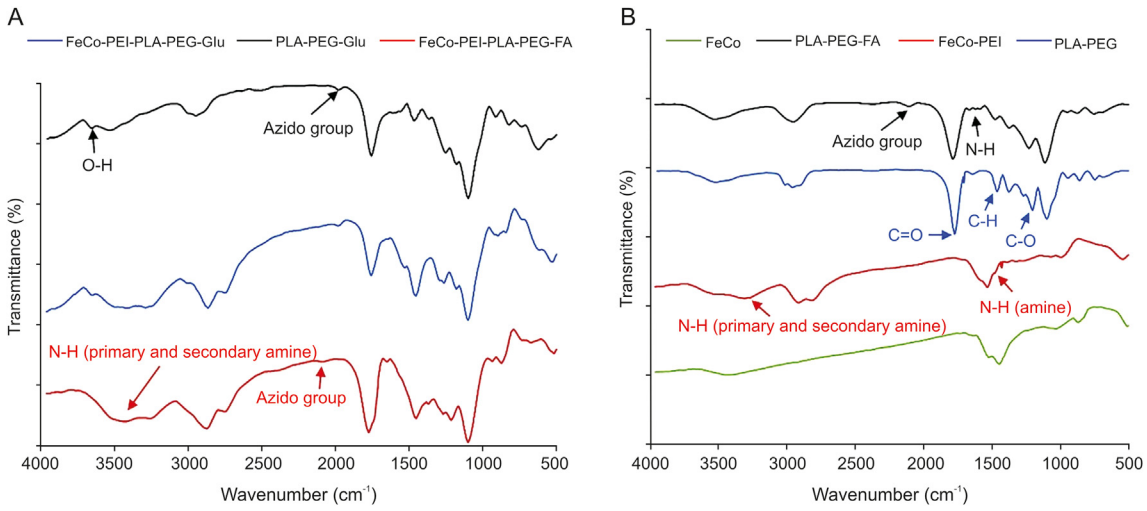

Fig. 2. FTIR spectrum of (A) FeCo-PEI-PLA-PEG-Glu, PLA-PEG-Glu and FeCo-PEI-PLA-PEG-FA and (B) FeCo, PLA-PEG-FA, FeCo-PEI and PLA-PEG. PLA: polylactic acid; PEG: polyethylene glycol; PEI: polyethylene imine; FA: folic acid; Glu: glucose.

2.9. Statistical analysis

The acquired data were analyzed using SPSS software version 20 (SPSS Inc. Chicago, US). The results of treated and control groups were compared by one-way ANOVA and post hoc test. All of the results are shown as means ± standard deviation values (SD). Significance was set at $P < 0.05$. Asterisks (*) indicates significant differences from the control group ($*P < 0.05$, $**P < 0.01$) and squares ($^{\#}$) indicate significant differences between the nanoparticles ($^{\#}P < 0.05$, $^{\#\#}P < 0.01$).

3. Results and discussion

3.1. Synthesis of PLA-PEG-FA and PLA-PEG-Glu copolymers

The chemical structure of the PLA-PEG-FA and PLA-PEG-Glu copolymers was examined with proton nuclear magnetic resonance spectroscopy (^{1}H NMR). Fig. 1 shows the ^{1}H NMR spectrum of PEI-PLA-PEG-FA copolymer, where the presence of CH_2 protons of PEG in PEI-PLA-PEG-FA copolymer was observed around 3.6 ppm (-CH_2CH_2O-). Moreover, the appearance of signals at 5.1 and 1.6 ppm is attributed to the methine (CH) protons and methyl protons – (CH_3) of PLA, respectively (Fig. 1A) [4].

The appearance of chemical shifts at 6.5–8.6 ppm (aromatic protons associated with FA) and 7.9 ppm (s, weak, ^{1}H, triazoles) provided evidence for successfully obtaining PEI-PLA-PEG-FA copolymer [47](Fig. 1A).

Also in Fig. 1B the multiple sharp peaks at 3.6–3.8 ppm and weak peak at 5.4 ppm which were assigned to methylene protons in PEG and aromatic proton in Glu respectively appeared on the spectrum after the reaction of PLA-PEI with PEG-Glu (Fig. 1B) [48].

The structures of PLA-PEG-FA and PLA-PEG-Glu were ascertained by the FTIR spectrum (Fig. 2). The sharp peak appearing at 1767 cm^{-1} was assigned to the carbonyl (C=O) group in the PLA-PEG copolymer [49]. The peaks that appeared in the regions of 1193 cm^{-1} and 1460 cm^{-1} are related to the stretching of C-O and the bending of -CH_2- groups in PLA-PEG copolymer, respectively [50]. Moreover, the peaks at 1640 and 1095 cm^{-1} corresponding to the C=O and C-O-C stretching of COOH in the FTIR spectrum of PEG, PLA- PEG-FA and PLA-PEG-Glu suggested that PEG was grafted to the nanoparticles [51]. The FTIR spectra of PLA-PEG-FA copolymer showed that there was a broad peak in the region between 1580 and 1648 cm^{-1} belonging to the amine group of FA. Moreover, the peak observed around 2108 and 2116 cm^{-1} were derived from azido group of FA and Glu, respectively. The peak at 3580 cm^{-1} corresponding to the O-H stretching of OH in the FTIR spectrum of Glu suggested that Glu was successfully grafted to the PLA-PEG.

The FTIR spectra of FeCo, FeCo-PEI, FeCo-PEI-PLA-PEG-FA, and FeCo-PEI-PLA-PEG-Glu are illustrated in Fig. 2.

After conjugation of PEI with FeCo nanoparticles, the PEI peaks from 1050 cm^{-1} to 1250 cm^{-1} were attributed to the amide and amide amino groups, which indicated that the PEI was attached on the surface of FeCo nanoparticles (Fig. 2) [41].

As also evident in Fig. 2, almost all peaks related to PLA-PEG, FeCo-PEI, Glu and FA were observed in the NPsA and NPsB; therefore, it indicated the successful synthesis of these nanoparticles.

Thermogravimetric analysis (TGA) of NPsA and NPsB was performed to find out different chemical compounds in the samples. The TGA curves of PEG, PEI, PLA, PLA-PEG, PLA-PEG-FA and PLA-PEG-Glu-FA copolymers are shown in Fig. 3.

TGA of the pure polymers (PEI, PLA and PEG) shows single step degradation while the spectrum of PLA-PEG copolymer exhibits three steps degradation related to the presence of three components in the PLA-PEG copolymer. The initial mass loss in the range of 175 °C to 305 °C might be due to the loss of adsorbed water molecules from the copolymer.

The second stage of the PLA-PEG degradation occurs between 320 °C and 380 °C, which is related to the thermal degradation reaction of the PLA polymer. The third stage of thermal degradation that occurs at temperatures above 380 °C is associated with degradation of PEG polymer [52].

The thermogram of the PLA-PEG-FA and PLA-PEG-Glu shows several mass losses during the temperature rise from 200 to 600 °C, which suggested that the Glu had a higher temperature resistance, compared to other pure PEI, PEG, PLA and FA; therefore, temperature resistance of PLA-PEG copolymer increased after binding to Glu.

As is seen in Fig. 3, the FeCo-PEI nanoparticles have a much better thermal stability than that of PLA-PEG-FA and PLA-PEG-Glu. Therefore, improvement in temperature resistance of PLA-PEG-FA and PLA-PEG-Glu was observed after modification with FeCo nanoparticles, which indicated the successful conjugation of PLA-PEG-FA and PLA-PEG-Glu with FeCo.

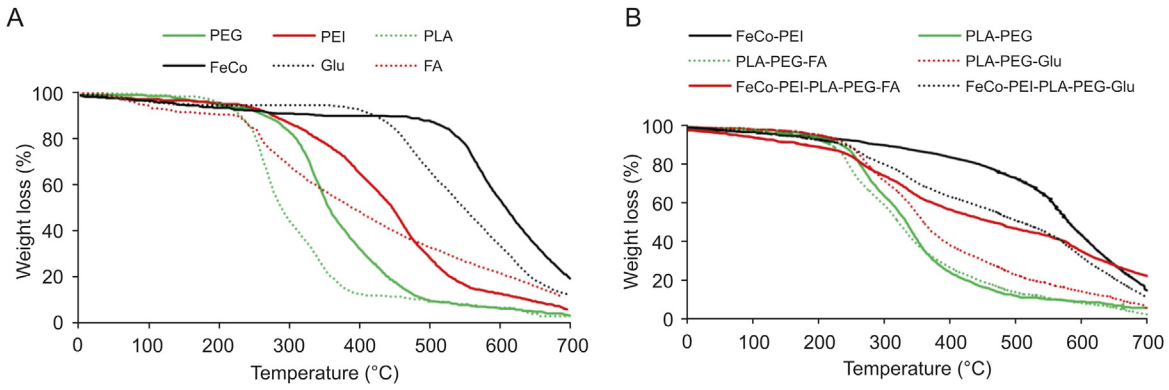

Fig. 3. TGA thermograms of (A) PEG, PEI, PLA, FeCo, Glu and FA and (B) FeCo-PEI, PLA-PEG, PLA-PEG-FA, PLA-PEG-Glu, FeCo-PEI-PLA-PEG-FA and FeCo-PEI-PLA-PEG-Glu. PLA: polylactic acid; PEG: polyethylene glycol; PEI: polyethylene imine; FA: folic acid; Glu: glucose.

3.2. Preparation and characterization of nanoparticles

The results of DLS indicated that there was no significant difference between the particle size of NPsA, NPsB and NPsAB (the hydrodynamic diameter of NPsA, NPsB and NPsAB was about 82, 94 and 88 nm, respectively). However, the hydrodynamic diameter of the nanoparticles increased after being conjugated with siRNA and PTX (Fig. 4). For example, the particle size of the NPsA increased from 88 nm to 120 nm after being encapsulated with siRNA and PTX. The surface charge of NPsA, NPsB and NPsAB was significantly reduced after being encapsulated with siRNA and PTX. It seems that the negative charge of phosphate backbone of the siRNA led to the decrease in the charge of the nanoparticles. A previous study found that the nanoparticles with a slightly negative surface charge and average particle sizes ranging between 100 and 150 nm have much higher transfer efficiency than larger nanoparticles [53,54]. Although nanoparticles smaller than 100 nm may have higher transfection efficiency than nanoparticles larger than 100 nm but the high nonspecific uptake of these nanoparticles could increase the side effects on healthy tissue [55].

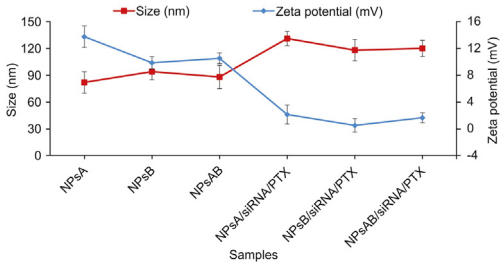

Fig. 4. The particle size and zeta potential of the both siRNA/PTX encapsulated and blank nanoparticles. NPsA: FeCo-PEI-PLA-PEG-FA nanoparticle; NPsB: FeCo-PEI-PLA-PEG-Glu nanoparticle; NPsAB: FeCo-PEI-PLA-PEG-FA/Glu nanoparticles; PTX: paclitaxel.

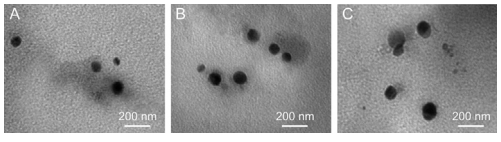

Fig. 5. TEM images of (A) NPsA/siRNA/PTX, (B) NPsB/siRNA/PTX and (C) NPsAB/siRNA/PTX nanoparticles. NPsA: FeCo-PEI-PLA-PEG-FA nanoparticle; NPsB: FeCo-PEI-PLA-PEG-Glu nanoparticle; NPsAB: FeCo-PEI-PLA-PEG-FA/Glu nanoparticles; PTX: paclitaxel.

The transmission electron microscopy (TEM) of the nanoparticles showed that the NPsA/siRNA/PTX, NPsB/siRNA/PTX and NPsAB/siRNA/PTX nanoparticles have spherical shape with uniform size distribution and smooth surface (Fig. 5). There was no significant difference between the morphology of the nanoparticles. The results also showed that the average size of the nanoparticles was about 100 nm. These results were consistent with DLS data (Fig. 4).

3.3. Magnetic property determination

Saturation magnetization of nanoparticles ranged from 70.6 to 165.2 emu/g. The FeCo nanoparticles showed high saturation magnetization (165.2 emu/g); however, these quantities decreased after coating FeCo with PEI. The values for saturation magnetization of FeCo and FeCo-PEI were determined as 165.2 and 131.4 emu/g, respectively (Fig. 6A).

The saturation magnetization values for NPsA, NPsB, and NPsAB were lower than those of the FeCo and FeCo-PEI nanoparticles (99.41, 107.84 and 94.8 emu/g for NPsA, NPsB, and NPsAB, respectively) (Fig. 6A). Such attenuation pattern of saturation magnetization is often seen in nanoparticles after coating the nanoparticles with non-magnetic compounds [56]. In general, the saturation magnetization of nanoparticles was reduced with encapsulation of siRNA and PTX into NPsA, NPsB and NPsAB (Fig. 6A). However, there was no significant difference between the magnetic properties of the nanoparticles after PTX and siRNA encapsulation. Magnetite properties of nanoparticles are an important factor in imaging and targeting using magnetic nanoparticles. Previous studies showed that nanoparticles with magnetite properties up to 9 emu/g are suitable for use in imaging and targeting nanoparticles [57]. Therefore, it seems that the nanoparticles synthesized in this experiment appear to be suitable for such purposes.

3.4. Drug encapsulation and release properties

The results of siRNA-FAM and PTX encapsulation efficiency in NPsA, NPsB and NPsAB are shown in Fig. 6B. Generally, the encapsulation efficiency of siRNA-FAM was significantly higher than that of PTX. The encapsulation efficiency of siRNA-FAM in various nanoparticles was in the range of 78% to 85% while in the case of PTX, it was in the range of 38% to 42%. There was no significant difference between encapsulation efficiency of the nanoparticles in each group (Fig. 6B). The maximum difference between the high and low encapsulation efficiency values of siRNA-FAM and PTX loaded samples was 7% and 4%, respectively (Fig. 6B). It seems that electrostatic interactions between the negative charge of

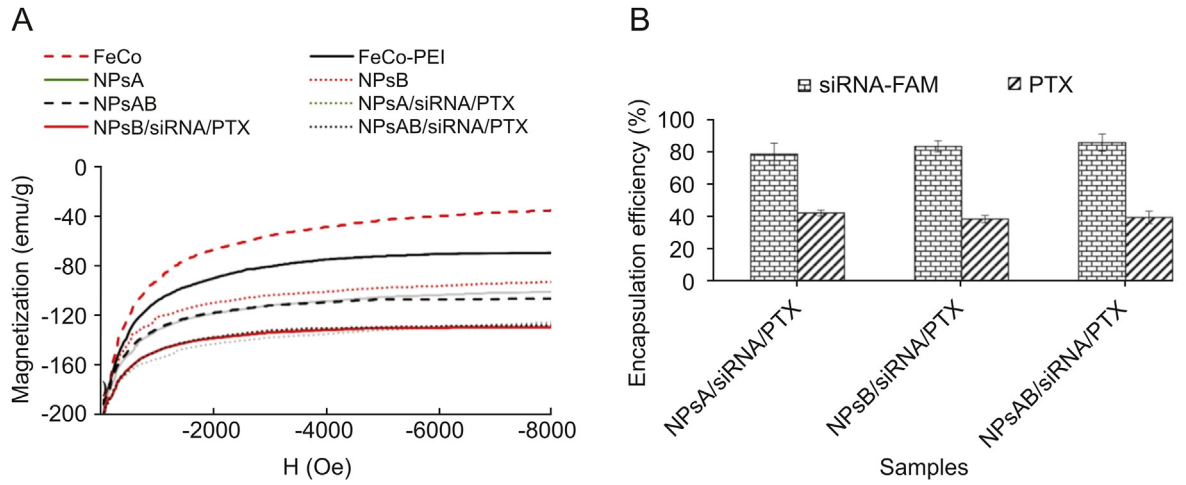

Fig. 6. (A) Magnetic behavior and (B) the percentage of PTX and siRNA-FAM encapsulated in different nanoparticles. NPsA: FeCo-PEI-PLA-PEG-FA nanoparticle; NPsB: FeCo-PEI-PLA-PEG-Glu nanoparticle; NPsAB: FeCo-PEI-PLA-PEG-FA/Glu nanoparticles; PTX: paclitaxel.

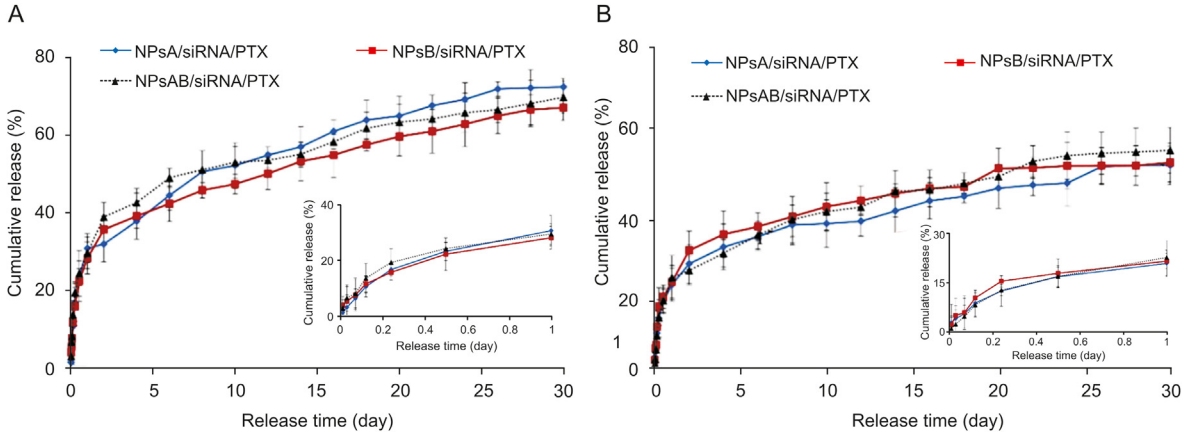

Fig. 7. (A) PTX and (B) siRNA release profiles from different nanoparticles in PBS buffer (pH=7.4) (Mean ± standard deviation) ($n = 3$). NPsA: FeCo-PEI-PLA-PEG-FA nanoparticle; NPsB: FeCo-PEI-PLA-PEG-Glu nanoparticle; NPsAB: FeCo-PEI-PLA-PEG-FA/Glu nanoparticles; PTX: paclitaxel.

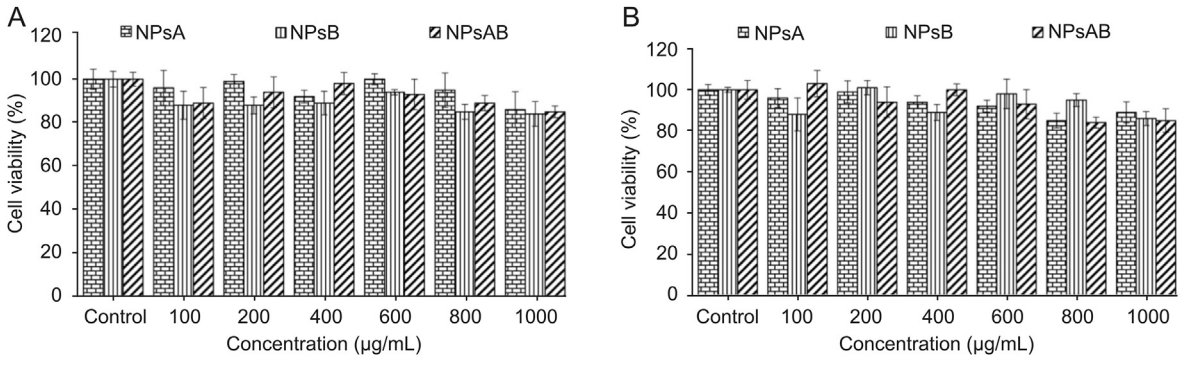

Fig. 8. The effects of different nanoparticles on viability of breast cancer cell lines (A) MCF-7 and (B) BT-474 cells (Mean ± standard deviation) ($n = 3$), NPsA: FeCo-PEI-PLA-PEG-FA nanoparticle; NPsB: FeCo-PEI-PLA-PEG-Glu nanoparticle; and NPsAB: FeCo-PEI-PLA-PEG-FA/Glu nanoparticles.

siRNA-FAM molecules and the positive charge of PEI in the nanoparticles are responsible for the increased values of siRNA-FAM encapsulation efficiency compared to PTX.

There was no significant difference between release behavior of PTX and also siRNA from NPsA/siRNA/PTX, NPsB/siRNA/PTX and NPsAB/siRNA/PTX nanoparticles. However, the cumulative release percentage of siRNA was found to be significantly lower than that of PTX after 30 days of incubation at 37 °C in PBS buffer (Fig. 7). It seems that the electrostatic interaction between siRNA and PEI of the nanoparticles may be responsible for this phenomenon [58,59]. Therefore, it is plausible that electrostatic interactions between the phosphate groups of siRNA and the NH_2 groups of the nanoparticles

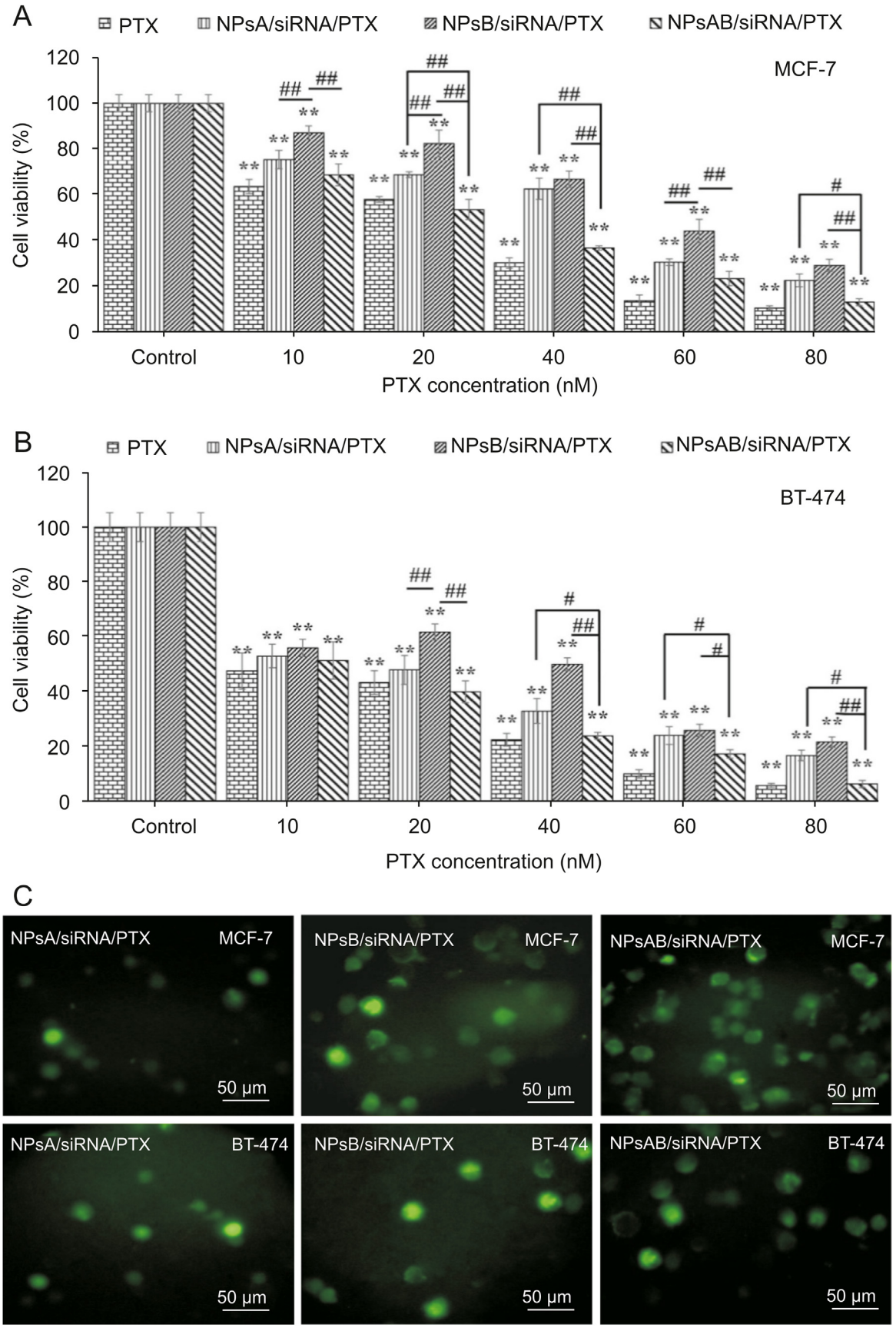

Fig. 9. (A and B) the anticancer effect and (C) fluorescence microscopy images of MCF-7 and BT-474 cells treated with different nanoparticles after 48 h incubation (Mean ± standard deviation) ($n = 3$). Asterisks ($^{*}P < 0.05$, $^{**}P < 0.01$) indicate significant differences from the control group, and squares ($^{\#}P < 0.05$, $^{\#\#}P < 0.01$) indicate significant differences between the nanoparticles, NPsA: FeCo-PEI-PLA-PEG-FA nanoparticle; NPsB: FeCo-PEI-PLA-PEG-Glu nanoparticle; NPsAB: FeCo-PEI-PLA-PEG-FA/Glu nanoparticles; PTX: paclitaxel.

resulted in a reduction in the release rate of siRNA from the nanoparticles.

The PTX and siRNA release from the nanoparticles was observed in two different stages. In the first stage, more than 50% of the PTX was released in the first three days. It was found that the rate of PTX release decreased significantly with increased incubation time more than three days. A similar release pattern was observed for siRNA.

The drug release pattern with initial burst release and consequently sustained release was observed in many micellar nanoparticles according the previous reports [60–63]. The drug may be encapsulated in different layers of the nanoparticles during the encapsulation process. The drugs encapsulated on the outer layer of the nanoparticles release more rapidly due to their exposure to the polar aqueous medium. While the drugs present in the inner part of the hydrophobic layer need more time to release from nanoparticles to aqueous environment. Some side effects, such as non-specific absorption and toxicity associated with high doses of the drug, may be caused by the injection of free drugs. Similar side effects may be seen in drug-loaded nanoparticles due to the explosive release of the drug from them. However, even in the explosive release step of drug, there is more time for drugs encapsulated in the nanoparticles to reach the targeted tissue compared to free drug. The reason for the sustained release of DNA from the PLA-PEG-PLA/DNA nanoparticles has been reported due to the hydrophobic PLA segment according to the previous report [36]. Abebe et al. [36] reported that the hydrophobic PLA inner shell formed an impermeable barrier which acted as an effective shield to protect DNA at neutral pH. Interestingly, lowering the pH from 7.4 to 4.5 led to a significant change in the release behavior. They reported that the low stability and quick degradation of the PLA-PEG copolymer under acidic conditions are the main causes of the rapid release of the DNA from PLA-PEG-PLA nanoparticles in the acidic environment. Considering what is mentioned above, it seems that the NPsA, NPsB and NPsAB nanoparticles have a high ability to provide drug release under acidic conditions of tumor tissue. However, due to hydrophobic nature of inner layers of prepared nanoparticles, a relatively significant fraction of loaded drug is not able to release from the carrier, so the maximum level of released drug is limited to about 60%.

3.5. In vitro cytotoxicity and transfection assay

In vitro cytotoxicity of blank nanoparticles and siRNA-FAM/PTX encapsulated nanoparticles were compared after 48 h. As is seen in Fig. 8, the siRNA/PTX-free nanoparticles (NPsA, NPsB, and NPsAB) showed good biocompatibility, and no remarkable cytotoxicity was observed after 48 h of incubation with MCF-7 and BT-474 cell lines. However, its toxicity significantly increased after encapsulation of siRNA/PTX in the nanoparticles (NPsA/siRNA/PTX, NPsB/siRNA/PTX, and NPsAB/siRNA/PTX) (Figs. 9A and B).

Given the fact that the siRNA-FAM has shown no significant effect on the cell viability of MCF-7 and BT-474 cell lines (results not shown), it can be concluded that the decrease in cell viability might be due to the effect of PTX on MCF-7 and BT-474 cells. The IC_{50} value of PTX-encapsulated in NPsAB/siRNA nanoparticles was significantly lower than that of NPsA/siRNA/PTX and NPsB/siRNA/PTX in MCF-7 cells after 48 h of incubation. The IC_{50} value of PTX-encapsulated in NPsAB/siRNA nanoparticles (NPsAB/siRNA/PTX) was 36.71 nM, while this amount was 45.27 nM and 55.67 nM for NPsA/siRNA/PTX and NPsB/siRNA/PTX, respectively. The similar trend was observed for BT-474 cells. The results showed that the BT-474 cells were more sensitive to the PTX than the MCF-7 cells. MTT analysis indicated that the cell viability of BT-474 cells was reduced to 50% after treatment with 20.15 nM of PTX for 48 h while this value was about 30.76 nM of PTX for MCF-7 cells at the same time of incubation (Table 1). Moreover, the results showed that NPsA (FeCo-PEI-PLA-PEG-FA)/siRNA/PTX nanoparticles had more effective antitumor activity than NPsB/siRNA/PTX nanoparticles. It has been known for decades that the metabolism of malignant cells is accompanied with significant increase in glycolysis level compared to normal tissues [9,10,64]. Since tumors undergo more proliferative processes than normal tissues, they need more Glu. Moreover, the requirement for folates (FA) in nucleotide synthesis has been confirmed in previous studies [8]. Our results indicated that NPsA/siRNA/PTX nanoparticles showed more effective antitumor activity than NPsB/siRNA/PTX nanoparticles. As mentioned above, it seems that the cancer cells need more FA to synthesize DNA due to its high rate of division. Therefore, FA-coated nanoparticles (NPsA) are absorbed more quickly than Glu-coated nanoparticles (NPsB) to breast cancer cells. Interestingly, the antitumor effects of the NPsAB/siRNA/PTX nanoparticles were significantly higher than those of NPsA/siRNA/PTX and NPsB/siRNA/PTX. The probable reasons may be as follows: First, since the nanoparticles were targeted to the breast cancer cells using two different ligands, there are more receptors on the cells' surface to absorb the nanoparticles compared to when the nanoparticles were targeted using a single ligand. Second, the amount of each type of receptors on the cancer cells is limited. So the surface receptors on the cancer cells are rapidly saturated by nanoparticles when only one type of ligand is used for the synthesis of the targeted nanoparticles. The targeted delivery of the drug to cancer cells decreases after the saturation of cell surface receptors by nanoparticles. In addition, the accumulation of nanoparticles in the normal tissues after the saturation of cell surface receptors may increases the toxicity of nanoparticles.

Table 1
The 50% inhibitory concentration (IC_{50}) values of free PTX and PTX encapsulated in different nanoparticles against MCF-7 and BT-474 cell lines after 48 h incubation.

Cell lines	PTX	NPsA/siRNA/PTX	NPsB/siRNA/PTX	NPsAB/siRNA/PTX
MCF-7	30.76	45.27	55.67	36.71
BT-474	23.15	30.08	38.1	24.41

NPsA: FeCo-PEI-PLA-PEG-FA nanoparticle; NPsB: FeCo-PEI-PLA-PEG-Glu nanoparticle; NPsAB: FeCo-PEI-PLA-PEG-FA/Glu nanoparticles; PTX: paclitaxel.

Fluorescence microscopy was used to evaluate the ability of the nanoparticles for co-delivery of DNA and drug into MCF-7 and BT-474 cell lines (Figs. 9C).

Fig. 9C shows fluorescence images of MCF-7 and BT-474 cells after 48 h of incubation with NPsA/siRNA/PTX, NPsB/siRNA/PTX and NPsAB/siRNA/PTX nanoparticles. The fluorescence emission observed within the cells indicated the ability of the nanoparticles to transfer siRNA-FAM into MCF-7 and BT-474 cells. Moreover, the circular morphology of MCF-7 cells after incubation with the nanoparticles may occur after the induction of apoptosis in MCF-7 and BT-474 cells by NPsA/siRNA/PTX, NPsB/siRNA/PTX and NPsAB/siRNA/PTX.

4. Conclusions

In this study, conjugated copolymers of NPsAB/siRNA/PTX were successfully synthesized for targeted gene delivery to breast cancer cells. Their chemical structures were confirmed through NMR and FTIR analysis and magnetic properties determination. The results obtained from TEM and DLS revealed that the nanoparticles have spherical morphology, with the hydrodynamic diameter in the range of 100-150 nm, which is suitable for intravenous injection and in vivo applications. Invitro drug release showed a sustained release manner of PTX and siRNA; however, the cumulative release

of PTX is higher than siRNA. The cytotoxicity assay demonstrated no significant toxicity of unloaded nanoparticles on MCF-7 and BT-474 cells, but siRNA/PTX loaded nanoparticles caused significant toxicity. In addition, the ability of NPsAB to improve the transfection efficiency was confirmed through increased uptake of siRNA-FAM in MCF-7 and BT-474 cells via fluorescence microscopy imaging.

Declaration of competing interest

The authors declare that there are no conflicts of interest.

Acknowledgments

This study has been supported by the Deputy Research and Technology, Ardabil University of Medical Sciences.

References

[1] R.I. Al-Wabli, T.M.M.H. Sakr, et al., Platelet-12 lipoxygenase targeting via a newly synthesized curcumin derivative radiolabeled with technetium-99m, Chem. Cent. J. 10 (2016), 73.
[2] S. Yang, W. Li, H. Sun, et al., Resveratrol elicits anti-colorectal cancer effect by activating miR-34c-KITLG in vitro and in vivo, BMC Canc. 15 (2015), 969.
[3] X. Deng, Q. Qiu, B. Yang, et al., Synthesis and biological evaluation of novel peptides with anti-cancer and drug resistance-reversing activities, Eur. J. Med. Chem. 89 (2015) 540–548.
[4] X. Liang, J. Fan, Y. Zhao, et al., A targeted drug delivery system based on folic acid-functionalized upconversion luminescent nanoparticles, J. Biomater. Appl. 9 (2017) 1247–1256.
[5] G.L. Zwicke, G.A. Mansoori, C.J. Jeffery, Targeting of cancer nanotherapeutics, Nano Rev. 1 (2012) 1–11.
[6] Y.-I. Kim, Folate and carcinogenesis: evidence, mechanisms, and implications, J. Nutr. Biochem. 10 (1999) 66–88.
[7] J.B. Mason, Folate: Effects on Carcinogenesis and the Potential for Cancer Chemoprevention, 1996.
[8] A. Garcia-Bennett, M. Nees, B. Fadeel, In search of the Holy Grail: folate-targeted nanoparticles for cancer therapy, Biochem. Pharmacol. 81 (2011) 976–984.
[9] L.G. Baggetto, Deviant energetic metabolism of glycolytic cancer cells, Biochimie 74 (1992) 959–974.
[10] O. Warburg, K. Posener, E. Negelein, The metabolism of cancer cells, Biochem. Z. 152 (1924) 319–344.
[11] O. Warburg, F. Wind, E. Negelein, The metabolism of tumors in the body, J. Gen. Physiol. 8 (1927) 519–530.
[12] J. Li, F.-K. Ma, Q.-F. Dang, et al., Glucose-conjugated chitosan nanoparticles for targeted drug delivery and their specific interaction with tumor cells, Front. Mater. Sci. 8 (2014) 363–372.
[13] V. Mamaeva, R. Niemi, M. Beck, et al., Inhibiting notch activity in breast cancer stem cells by glucose functionalized nanoparticles carrying $γ$-secretase inhibitors, Mol. Ther. 24 (2016) 926–936.
[14] M. Wang, M. Thanou, Targeting nanoparticles to cancer, Pharmacol. Res. 62 (2010) 90–99.
[15] G.-F. Hao, G.-F. Yang, C.-G. Zhan, Structure-based methods for predicting target mutation-induced drug resistance and rational drug design to overcome the problem, Drug Discov. Today 17 (2012) 1121–1126.
[16] F. Kanzawa, K. Nishio, T. Ishida, et al., Anti-tumour activities of a new benzo [c] phenanthridine agent, 2, 3-(methylenedioxy)-5-methyl-7-hydroxy-8-methoxybenzo [c] phenanthridinium hydrogensulphate dihydrate (NK109), against several drug-resistant human tumour cell lines, Br. J. Canc. 76 (1997) 571–581.
[17] Q. He, J. Liu, X. Sun, et al., Preparation and characteristics of DNA-nanoparticles targeting to hepatocarcinoma cells, World J. Gastroenterol. 10 (2004) 660–663.
[18] A. Camirand, Y. Lu, M. Pollak, Co-targeting HER2/ErbB2 and insulin-like growth factor-1 receptors causes synergistic inhibition of growth in HER2-overexpressing breast cancer cells, Med. Sci. Mon. Int. Med. J. Exp. Clin. Res. 8 (2002) BR521–BR526.
[19] M. Mancini, M.B. Gariboldi, E. Taiana, et al., Co-targeting the IGF system and HIF-1 inhibits migration and invasion by (triple-negative) breast cancer cells, Br. J. Canc. 110 (2014) 2865–2873.
[20] M. Kumar, M. Yigit, G. Dai, et al., Image-guided breast tumor therapy using a small interfering RNA nanodrug, Canc. Res. 70 (2010) 7553–7561.
[21] Y. Patil, J. Panyam, Polymeric nanoparticles for siRNA delivery and gene silencing, Int. J. Pharm. 367 (2009) 195–203.
[22] S.F. Peng, H.K. Hsu, C.C. Lin, et al., Novel PEI/Poly-γ-gutamic acid nanoparticles for high efficient siRNA and plasmid DNA co-delivery, Molecules 22 (2017), 86.
[23] X.Z. Yang, S. Dou, T.M. Sun, et al., Systemic delivery of siRNA with cationic lipid assisted PEG-PLA nanoparticles for cancer therapy, J. Contr. Release 156 (2011) 203–211.
[24] S. Kapse-Mistry, T. Govender, R. Srivastava, et al., Nanodrug delivery in reversing multidrug resistance in cancer cells, Front. Pharmacol. 5 (2014), 159.
[25] Y. Yang, H. Zhao, Y. Jia, et al., A novel gene delivery composite system based on biodegradable folate-poly (ester amine) polymer and thermosensitive hydrogel for sustained gene release, Sci. Rep. 6 (2016), 21402.
[26] J. Hu, M. Zhu, K. Liu, et al., A biodegradable polyethylenimine-based vector modified by trifunctional peptide R18 for enhancing gene transfection efficiency in vivo, PloS One 11 (2016), e0166673.
[27] S. Shi, X. Zhu, Q.F. Guo, et al., Self-assembled mPEG-PCL-g-PEI micelles for simultaneous codelivery of chemotherapeutic drugs and DNA: synthesis and characterization in vitro, Int. J. Nanomed. 7 (2012) 1749–1759.
[28] A. Amani, T. Kabiri, S. Shafiee, et al., Preparation and characterization of PLA-PEG-PLA/PEI/DNA nanoparticles for improvement of transfection efficiency and controlled release of DNA in gene delivery systems, Iran, J. Pharm. Res. IJPR. 18 (2019) 125–141.
[29] L. Chen, F. Ji, Y. Bao, et al., Biocompatible cationic pullulan-g-desoxycholic acid-g-PEI micelles used to co-deliver drug and gene for cancer therapy, Mater. Sci. Eng. C 70 (2017) 418–429.
[30] S. Shi, K. Shi, L. Tan, et al., The use of cationic MPEG-PCL-g-PEI micelles for co-delivery of Msurvivin T34A gene and doxorubicin, Biomaterials 35 (2014) 4536–4547.
[31] J. Shen, Q. Yin, L. Chen, et al., Co-delivery of paclitaxel and survivin shRNA by pluronic P85-PEI/TPGS complex nanoparticles to overcome drug resistance in lung cancer, Biomaterials 33 (2012) 8613–8624.
[32] S. Biswas, P.P. Deshpande, G. Navarro, et al., Lipid modified triblock PAMAM-based nanocarriers for siRNA drug co-delivery, Biomaterials 34 (2013) 1289–1301.
[33] C. Perez, A. Sanchez, D. Putnam, et al., Poly(lactic acid)-poly(ethylene glycol) nanoparticles as new carriers for the delivery of plasmid DNA, J. Contr. Release 75 (2001) 211–224.
[34] J. Lu, X. Chuan, H. Zhang, et al., Free paclitaxel loaded PEGylated-paclitaxel nanoparticles: preparation and comparison with other paclitaxel systems in vitro and in vivo, Int. J. Pharm. 471 (2014) 525–535.
[35] J. Wang, C.-F. Xu, A. Liu, et al., Delivery of siRNA with nanoparticles based on PEG–PLA block polymer for cancer therapy, Nanomed. Nanotechnol. Biol. Med. 2 (2016) 464.
[36] D.G. Abebe, R. Kandil, T. Kraus, et al., Three-layered biodegradable micelles prepared by two-step self-assembly of PLA-PEI-PLA and PLA-PEG-PLA triblock copolymers as efficient gene delivery system, macromol, Biosci 15 (2015) 698–711.
[37] K. Yan, H. Li, P. Li, et al., Self-assembled magnetic fluorescent polymeric micelles for magnetic resonance and optical imaging, Biomaterials 35 (2014) 344–355.
[38] Y. Chen, K. Ai, J. Liu, et al., Multifunctional envelope-type mesoporous silica nanoparticles for pH-responsive drug delivery and magnetic resonance imaging, Biomaterials 60 (2015) 111–120.
[39] J. Liu, T. Wei, J. Zhao, et al., Multifunctional aptamer-based nanoparticles for targeted drug delivery to circumvent cancer resistance, Biomaterials 91 (2016) 44–56.
[41] L. Zhang, Y. Li, J.C. Yu, et al., Redox-responsive controlled DNA transfection and gene silencing based on polymer-conjugated magnetic nanoparticles, RSC Adv. 6 (2016) 72155–72164.
[42] A. Amani, J.M. Begdelo, H. Yaghoubi, et al., Multifunctional magnetic nanoparticles for controlled release of anticancer drug, breast cancer cell targeting, MRI/fluorescence imaging, and anticancer drug delivery, J. Drug Deliv. Sci. Technol. 49 (2019) 534–546.
[43] S.J.T. Rezaei, H.S. Abandansari, M.R. Nabid, et al., pH-responsive unimolecular micelles self-assembled from amphiphilic hyperbranched block copolymer for efficient intracellular release of poorly water-soluble anticancer drugs, J. Colloid Interface Sci. 425 (2014) 27–35.
[44] A.F.M. El-Mahdy, T. Shibata, T. Kabashima, et al., Delivery of siRNA using siRNA/cationic vector complexes encapsulated in dendrimer-like polymeric DNAs, RSC Adv. 5 (2015) 32775–32785.
[45] W.M. Ibrahim, A.H. AlOmrani, A.E.B. Yassin, Novel sulpiride-loaded solid lipid nanoparticles with enhanced intestinal permeability, Int. J. Nanomed. 9 (2014) 129–144.
[46] Q. Wang, C. Li, T. Ren, et al., Poly (vinyl methyl ether/maleic anhydride)-doped PEG–PLA nanoparticles for oral paclitaxel delivery to improve bioadhesive efficiency, Mol. Pharm. 14 (2017) 3598–3608.
[47] S.-J. Yang, F.-H. Lin, K.-C. Tsai, et al., Folic acid-conjugated chitosan nanoparticles enhanced protoporphyrin IX accumulation in colorectal cancer cells, Bioconjugate Chem. 21 (2010) 679–689.
[48] F. Sadeghi, F. Hadizadeh, S. Sazmand, et al., Synthesis and self-assembly of biodegradable polyethylene glycol-poly (lactic acid) diblock copolymers as polymersomes for preparation of sustained release system of doxorubicin, Int. J. Pharm. Investig. 5 (2015) 134–141.
[49] H.-K. Jang, B.S. Kim, Molecular recognition properties of biodegradable photo-crosslinked network based on poly (lactic acid) and poly (ethylene glycol), Macromol. Res. 21 (2013) 370–375.
[50] B.W. Chieng, I.N. Azowa, W.M. Zin, et al., Effects of graphene nanopletelets on poly (lactic acid)/poly (ethylene glycol) polymer nanocomposites, Polymers 6 (2014) 93–104.
[51] T. Yildiz, R. Gu, S. Zauscher, et al., Doxorubicin-loaded protease-activated

near-infrared fluorescent polymeric nanoparticles for imaging and therapy of cancer, Int. J. Nanomed. 13 (2018) 6961–6986.
[52] M. Mariano, F. Pilate, F.B. de Oliveira, et al., Preparation of cellulose nanocrystal-reinforced poly (lactic acid) nanocomposites through non-covalent modification with PLLA-based surfactants, ACS Omega 2 (2017) 2678–2688.
[53] G.F. Liang, Y.L. Zhu, B. Sun, et al., PLGA-based gene delivering nanoparticle enhance suppression effect of miRNA in HePG2 cells, Nanoscale Res. Lett. 6 (2011), 447.
[54] S. Prabha, W.-Z. Zhou, J. Panyam, et al., Size-dependency of nanoparticle-mediated gene transfection: studies with fractionated nanoparticles, Int. J. Pharm. 244 (2002) 105–115.
[55] S.S. Yu, C.M. Lau, S.N. Thomas, et al., Size-and charge-dependent non-specific uptake of PEGylated nanoparticles by macrophages, Int. J. Nanomed. 7 (2012) 799–813.
[56] P. Pouponneau, J.-C. Leroux, S. Martel, Magnetic nanoparticles encapsulated into biodegradable microparticles steered with an upgraded magnetic resonance imaging system for tumor chemoembolization, Biomaterials 30 (2009) 6327–6332.
[57] Y. Zhuang, L. Zhao, L. Zheng, et al., Laponite-polyethylenimine based theranostic nanoplatform for tumor-targeting CT imaging and chemotherapy, ACS Biomater. Sci. Eng. 3 (2017) 431–442.
[58] Y. Wu, W. Wang, Y. Chen, et al., The investigation of polymer-siRNA nanoparticle for gene therapy of gastric cancer in vitro, Int. J. Nanomed. 5 (2010) 129–136.
[59] Y. Lee, S.H. Lee, J.S. Kim, et al., Controlled synthesis of PEI-coated gold nanoparticles using reductive catechol chemistry for siRNA delivery, J. Contr. Release 155 (2011) 3–10.
[60] N.H. Hoang, T. Sim, C. Lim, et al., A nano-sized blending system comprising identical triblock copolymers with different hydrophobicity for fabrication of an anticancer drug nanovehicle with high stability and solubilizing capacity, Int. J. Nanomed. 14 (2019) 3629–3644.
[61] N. Wang, Z. Wang, S. Nie, et al., Biodegradable polymeric micelles coencapsulating paclitaxel and honokiol: a strategy for breast cancer therapy in vitro and in vivo, Int. J. Nanomed. 12 (2017) 1499–1514.
[62] Y. Wang, Y. Li, Q. Wang, et al., Pharmacokinetics and biodistribution of polymeric micelles of paclitaxel with pluronic P105/poly (caprolactone) copolymers, Pharmazie 63 (2008) 446–452.
[63] L.-C. Cheng, Y. Jiang, Y. Xie, et al., Novel amphiphilic folic acid-cholesterol-chitosan micelles for paclitaxel delivery, Oncotarget 8 (2017) 3315–3326.
[64] T. Kong, J. Zeng, X. Wang, et al., Enhancement of radiation cytotoxicity in breast-cancer cells by localized attachment of gold nanoparticles, Small 4 (2008) 1537–1543.